submitted to *Physical Chemistry Chemical Physics*

Infrared Multiple Photon Dissociation Action Spectroscopy of Protonated Unsymmetrical Dimethylhydrazine and Proton-bound Dimers of Hydrazine and Unsymmetrical Dimethylhydrazine

Christopher P. McNary,[a] Maria Demireva,[a,†] Jonathan Martens,[b] Giel Berden,[b] Jos Oomens,[b,c] L. A. Hamlow,[d] M. T. Rodgers,[d] and P.B. Armentrout*[a]

[a] *Department of Chemistry, University of Utah, Salt Lake City, UT 84112, USA.*
[b] *Radboud University, Institute for Molecules and Materials, FELIX Laboratory, Toernooiveld 7, 6525ED Nijmegen, The Netherlands.*
[c] *Van't Hoff Institute for Molecular Sciences, University of Amsterdam, Science Park 904, 1098XH Amsterdam, The Netherlands.*
[d] *Department of Chemistry, Wayne State University, Detroit, Michigan 48202, United States*
[†] *Present address: Sandia National Laboratories, Livermore, CA, 94551, USA.*

Abstract. The gas-phase structures of protonated unsymmetrical 1,1-dimethylhydrazine (UDMH) and the proton-bound dimers of UDMH and hydrazine are examined by infrared multiple photon dissociation (IRMPD) action spectroscopy utilizing light generated by a free electron laser and an optical parametric oscillator laser system. To identify the structures present in the experimental studies, the measured IRMPD spectra are compared to spectra calculated at the B3LYP-GD3BJ/6-311+G(d,p) level of theory. These comparisons show that protonated UDMH binds the proton at the methylated nitrogen atom (α) with two low-lying α conformers probably being populated. For $(UDMH)_2H^+$, the proton is shared between the methylated nitrogen atoms with several low-lying α conformers likely to be populated. Higher-lying conformers of $(UDMH)_2H^+$ in which the proton is shared between α and β (unmethylated) nitrogen atoms cannot be ruled out on the basis of the IRPMD spectrum. For $(N_2H_4)_2H^+$, there are four low-lying conformers that all reproduce the IRMPD spectrum reasonably well. As hydrazine and UDMH see usage as fuels for rocket engines, such spectra are potentially useful as a means of remotely monitoring rocket launches, especially in cases of unsuccessful launches where environmental hazards need to be assessed.

Introduction

Hydrazine (N_2H_4) and unsymmetrical 1,1–dimethylhydrazine (commonly known as UDMH) find applications in several areas. They are molecules that can potentially act as clean chemical hydrogen storage systems.[1, 2] They have been used as a blowing agent in preparing polymer foams and can be precursors to catalysts and pharmaceuticals.[3] They are also used as fuels for some types of mono- and bipropellant rocket engines.[4] During successful and especially unsuccessful rocket burns,[4] these fuels are released into the atmosphere where they exothermically react with atmospheric gases, such as ozone and hydroxyl radical, creating potentially toxic compounds such as methylhydroperoxide, methyldiazene, and diazomethane.[5, 6] Additionally, during launch and reentry, ion-molecule reactions in the ionosphere can form protonated hydrazine, $N_2H_5^+$,[4] a species that can also form during ionization of hydrazine in water[7] and potentially under the harsh conditions of combustion. Furthermore, ionic liquids including hydrazinium salts have been explored as possible replacements for hydrazine fuels as they can remain energy dense but have lower volatility and are greener fuels.[8-10] Ionic liquids can be used for both chemical and electrical propulsion, where the latter process operates similarly to an electrospray ionization source and produces similar types of ions. In such systems, the hydrazine and UDMH can be intrinsically protonated, and typically would be when used with electrospray thrusters that are being advanced for micro and nanosatellite applications.[11-13]

Therefore, it is of interest to explore the fundamental properties of protonated hydrazine and UDMH and their clusters. In the present study, we examine the vibrational (infrared) spectra of such complexes, which are unexplored, to the best of our knowledge. These spectra may be of particular utility as a means of remotely monitoring rocket launches, especially for potential environmental hazard assessment in the troposphere during cases of unsuccessful rocket burns when unspent fuel is released in abundance. Although neutral species may be prevalent under such circumstances, the likely presence of some protonated species would affect the composite spectrum, making the spectra obtained here information needed for complete identification.

In previous studies, we have used guided ion beam tandem mass spectrometry and quantum

chemistry to explore the thermochemistry of protonated hydrazine and UDMH and their clusters.[14-16] Protonated hydrazine, $N_2H_5^+$, was observed to dissociate by homolytic and heterolytic N–N bond cleavages.[16] The thresholds for these processes showed that these dissociations occur along non-adiabatic pathways forming the excited NH_3^+ ($^2A_2''$) + NH_2 ($^2A_1$) and NH_2^+ ($^1A_1$) + NH_3 ($^1A_1$) product asymptotes, respectively.[16] For the $(N_2H_4)_nH^+$ clusters where n = 2 – 4, the primary dissociation pathway for all reactants consists of loss of a single hydrazine molecule followed by the sequential loss of additional hydrazine molecules at higher collision energies for n = 3 and 4, such that sequential binding energies could be ascertained.[15] In that study, a theoretical potential energy surface (PES) that links four low-energy conformers of the $(N_2H_4)_2H^+$ dimer was characterized. The proton-bound dimer of UDMH dissociates by loss of neutral UDMH, such that the dimer bond dissociation energy (BDE) could be measured. Eleven conformers of the dimer were located theoretically. Finally, the thermodynamics for hydration of protonated hydrazine and UDMH have also been examined by determining BDEs for loss of water from $(N_2H_4)H^+(H_2O)_n$, where n = 1 and 2, and $(UDMH)H^+(H_2O)$.[14]

A number of different theoretical approaches were utilized and yielded differing results in our previous work on the dissociation thermochemistry of $N_2H_5^+$,[16] $(N_2H_4)_nH^+$ clusters where n = 2 – 4 and $(UDMH)_2H^+$,[15] and hydrated systems, $(N_2H_4)H^+(H_2O)_n$ where n = 1 and 2 and $(UDMH)H^+(H_2O)$.[14] In the $N_2H_5^+$ system where covalent bonds are being cleaved, B3LYP did not perform well, but this system is small enough that CCSD(T) calculations could be performed and reproduced the observed (and literature) thermochemistry well. For the small proton bound clusters, M06 and PBE0 approaches yielded the best results (mean absolute deviations (MADs) from experiment of about 3 kJ/mol), whereas CCSD(T) had a MAD of ~6 kJ/mol, and B3LYP was ~9 kJ/mol. For the hydrated systems, CCSD(T) was the best (MAD ~ 1 kJ/mol), with B3LYP near 3 kJ/mol, and M06 and PBE0 near 5 kJ/mol. Potentially, the accuracy of these calculations can be checked by determining the correct global minimum structure of these complexes. The present work attempts to do this by employing infrared multiple photon dissociation (IRMPD) action spectroscopy to probe the structures of protonated UDMH and the proton-bound dimers of UDMH

and hydrazine. IRMPD action spectroscopy is a powerful tool for examining structure specific vibrational modes in the gas phase at room temperatures.[17-21]

Experimental and theoretical methods

Experimental methods. Experiments in the IR fingerprint region of 16.6 – 5.4 μm (600 – 1850 cm^{-1}) were performed at the Free Electron Lasers for Infrared eXperiments (FELIX) Facility at Radboud University, The Netherlands, using the FELIX-2 beam line.[22] In the 2800 to 3600 cm^{-1} range, experiments were performed at Wayne State University using IR light from a 10 Hz Nd:YAG pumped (Continuum Lasers, Surelite EX) table-top optical parametric oscillator/amplifier (OPO/A, LaserVision) laser. IRMPD spectra of $(UDMH)_2H^+$ and $(N_2H_4)_2H^+$ were recorded on an optically accessible Bruker AmaZon ETD quadrupole ion trap (QIT) mass spectrometer, at FELIX[23] and at Wayne State University (WSU).[24] The proton-bound dimer ions were generated in an ESI source using solutions acidified with HCl of 10 mM N_2H_4 or UDMH in H_2O at FELIX and 25 mM N_2H_4 in H_2O or 25 mM UDMH in 50:50 methanol:water at WSU. Ions in the trap are believed to be near room temperature because of rapid collisional cooling with He, as previously investigated.[25, 26] Once the selected ions were mass-isolated in the trap, the ions were irradiated with 2 – 10 macropulses of FELIX or 20 pulses of the OPO. Ion intensities were determined by scanning ions out of the trap onto a conversion dynode detector. For the present FELIX experiments, spectra were recorded over the spectral range of 600 – 1850 cm^{-1} (16.6 μm – 5.4 μm) with a 3 cm^{-1} step, which can be covered with a single setting of the electron beam energy of FELIX. For both FELIX and OPO studies, the fractional yield was determined as $Y = \sum I_F/(I_P + \sum I_F)$, where I_P and I_F are the integrated intensities of the precursor and fragment ion mass peaks, respectively. The IRMPD spectra were generated by plotting the yield as a function of the wavenumber of the IR radiation. A linear correction was applied to the yield to account for the frequency-dependent variation in the IR laser pulse energy.

Protonated UDMH could not be observed easily in the QIT because this species rapidly complexes to water, a problem avoided in a Fourier transform ion cyclotron resonance (FTICR)

mass spectrometer because it operates at much lower pressure. The 4.7 T FTICR MS at FELIX, described elsewhere,[19, 27, 28] was used to record the fingerprint region of the IRMPD spectrum of protonated UDMH. A solution of 10 mM UDMH in H_2O acidified with HCl was used with a flow rate of 10 – 25 μL min^{-1}. Ions generated in the Micromass Z-spray electrospray ionization (ESI) source were accumulated in a hexapole trap for 10 s before being extracted through a quadrupole bender and injected into the ICR cell via a radiofrequency (rf) octopole ion guide. To avoid collisional heating of the ions, instead of a gas pulse, ion capturing in the ICR cell was effected by temporally switching the dc bias of the octopole, thus re-referencing the kinetic energy of the ions to about 2V above the dc potential of the ICR cell (0 V).[21, 27, 29] The ions of interest were mass isolated using a stored waveform inverse Fourier transform (SWIFT) excitation pulse[30, 31] and allowed to cool radiatively for 0.4 s.[32] These ions were irradiated with light from FELIX for 8.5 s at a 10 Hz macropulse repetition rate. In order to increase the on-resonance dissociation yield, the ions were irradiated for 24 ms with the output of a 30 W continuous-wave CO_2 laser directly after each FELIX macropulse. No spectrum has been recorded in the hydrogen-stretching region because the OPO laser power is too low (compared to FELIX) to induce dissociation of H^+(UDMH).

Computational Details. Stable geometries, vibrational frequencies, and energies for the proton-bound dimers of hydrazine and UDMH were thoroughly investigated in previous studies,[15] where details can be found. Possible conformations of these species were explored via a simulated annealing procedure with further geometry optimizations performed at the B3LYP/6-31G(d) level of theory.[33, 34] Final geometry optimizations and vibrational frequency calculations were performed at the B3LYP-GD3BJ/6-311+G(d,p) level of theory, which includes empirical dispersion functions, the D3 version of Grimme dispersion[35] (GD3) with Becke–Johnson (BJ) damping. Vibrational frequencies obtained were scaled by 0.989 to obtain zero-point energy (ZPE) and free energy thermal corrections at 298 K. Single-point energy calculations with and without empirical dispersion were performed with a 6-311+G(2d,2p) basis set at B3LYP, M06,[36] PBE0,[37, 38] mPW1PW91,[33, 39, 40] and MP2(full)[41-45] (where full indicates correlation of all electrons) and

CCSD(T) levels using optimized geometries at the B3LYP-GD3BJ/6-311+G(d,p) level of theory. The empirical dispersion functions were set to GD3BJ for B3LYP and PBE0 and GD3[46] for M06 levels of theory.

Here, we performed additional calculations for UDMH(H^+). Single-point energy calculations were performed at the B3LYP-GD3BJ and MP2(full) (where full indicates correlation of all electrons)[41-45] levels with a 6-311+G(2d,2p) basis set. In addition, the restricted open-shell coupled cluster with single, double, and perturbative triple excitations, ROCCSD(T),[47-51] method with the correlation consistent basis set, aug-cc-pV*n*Z (*n* = D, T, and Q), was used to formulate two complete basis set (CBS) limits indicated as Feller CBS,[52] as outlined in previous work.[53]

The present work also calculated the vibrational spectrum of all species using the optimized structures at the B3LYP-GD3BJ/6-311+G(d,p) level of theory. For comparison to the experimental spectra, the vibrational frequencies were scaled by a variable factor and broadened by a 80 cm^{-1} full width at half maximum Gaussian line shape. This broadening accounts for the finite laser bandwidth, unresolved rotational structure of the ions (which should be near room temperature), anharmonicity of the vibrational modes, and broadening as a result of the multiple-photon absorption process. The multiple scaling factors used below were chosen to emphasize good agreement between calculated and experimentally well-resolved vibrational peaks, an approach consistent with previous IRMPD studies.[54-58] Although a single scaling factor could have been chosen, the resulting offsets would have deemphasized the otherwise good agreement in the shapes of the bands.

Results and discussion

Theoretical Structures. (UDMH)H^+. As noted above, the theoretical structures for (UDMH)H^+ were previously explored.[15] (UDMH)H^+ isomers are named with α designating protonation of the methylated nitrogen and β indicating protonation of the unmethylated nitrogen, with g (gauche, angles of 45 – 135°) and t (trans, 135 – 180°) designating the dihedral angle between the proton on N_α and the hydrogens on N_β. Two low-lying α isomers, α(g,g) and α(t,g),

and one higher-lying β isomer were located and are shown in Figure 1, with relative energies listed in Table 1. The α(g,g) conformer is the global minimum (GM) at 0 and 298 K at all levels of theory, with the α(t,g) conformer predicted to lie 1.3 – 2.9 and 1.2 – 2.7 kJ/mol higher in energy at those temperatures, respectively. It can be realized that there are two enantiomers of the α(t,g) conformer (coupled by rotation about the N–N bond), such that there are two equivalent structures available for population. At these small relative energies, Maxwell-Boltzmann populations at 298 K for the α(g,g) and α(t,g) isomers are 45 – 60% and 55 – 40%, respectively, such that both conformers are likely populated at room temperature. The transition state (TS) between these conformers lies 10 – 13 kJ/mol higher than the GM at 298 K. Because the average internal energy of the molecule at 298 K is 11.0 kJ/mol, it seems likely that these conformers may not readily interconvert at room temperature. The β isomer is much higher in energy, 29 – 35 kJ/mol, such that it should not be populated at 298 K.

Experimental IRMPD spectrum of (UDMH)H$^+$. Figure 1 shows the IRMPD spectrum of (UDMH)H$^+$ examined from 600 to 1800 cm^{-1}. The only observed photodissociation pathway of (UDMH)H$^+$ resulted in the loss of ammonia (NH_3). Unpublished collision-induced dissociation experiments verify that this is the lowest-energy dissociation channel. Note that the loss of NH_3 from the α isomers necessitates an intramolecular proton transfer, which can occur by first forming the β isomer and then passing over a TS that heterolytically breaks the N–N bond and synchronously transfers a hydrogen from a methyl group to N_α. The latter step is rate limiting and calculated to lie 210 – 234 kJ/mol above the GM. Alternatively, as the N–N bond is homolytically broken in one of the α conformers, transfer of a hydrogen atom from one of the methyl groups to N_β can also occur, with a TS lying 265 – 287 kJ/mol above the GM. In either case, the final products are $CH_3NHCH_2^+ + NH_3$. Deuterium labeling shows that the latter mechanism dominates.

The theoretical IR spectra of the two low-lying α conformers, Figure 1, reproduce the IRMPD spectrum with high fidelity if two scaling factors are used: 0.975 for frequencies between 600 and 1275 cm^{-1} and 0.955 for frequencies of 1275 – 1800 cm^{-1}, where the switching frequency is determined after scaling. In the lower frequency range, the two major bands observed both

correspond largely to the NH_2 umbrella motion coupled with the N–N stretch and a CH_3 bend at 867 and 1040 cm^{-1} for α(g,g) and 885 and 1017 cm^{-1} for α(t,g). Note that the splitting and relative intensities of these two experimental bands are better reproduced by the α(t,g) conformer. Further, the shoulder observed experimentally at 750 cm^{-1} is reproduced well by the α(t,g) conformer, whereas this band is 20 times less intense and shifted to 791 cm^{-1} for the GM α(g,g) conformer. In the higher frequency range, the two main peaks observed correspond to CH_3 bends and the NH_2 bend at 1430/1444 and 1605 cm^{-1} for the α(g,g) conformer and 1439/1441 and 1607 cm^{-1} for the α(t,g) conformer. Clearly, the β isomer does not reproduce the experimental spectrum well, no matter what scaling factors might be used. According to theory, both α(g,g) and α(t,g) should be populated at 298 K. Indeed, a Maxwell-Boltzmann population weighted IR spectrum reproduces the IRMPD spectrum reasonably well, consistent with the presence of both isomers.

Theoretical Structures. $(UDMH)_2H^+$. For $(UDMH)_2H^+$, the isomers are named by again designating the protonated nitrogen as α or β for the methylated and unmethylated N, respectively, with the addition of a donor (D) and acceptor (A) notation that indicates hydrogen-bonding interactions. The relative orientation of the two N–N UDMH bonds is then provided by designating the ∠NNNN dihedral angle by c (cis, for angles between 0 – 45°), g, and t designations. The four lowest energy $(D_\alpha)(A_\alpha)$ conformers are shown in Figure 2 with energies listed in Table 2. They all share the proton between the two α nitrogen atoms and lie within 3 kJ/mol of one another. The proton can also be shared between one methylated and one unmethylated nitrogen atom, $(D_\alpha)(A_\beta)$. Three conformers result and lie 3 – 12 kJ/mol higher in energy than the GM at 298 K. Sharing the proton between both unmethylated nitrogen atoms, $(D_\beta)(A_\beta)$, increases the energy further, in part because there can be no hydrogen bonding between the methylated nitrogen atoms. These three structures lie more than 18 kJ/mol above the GM. On the basis of the theoretical energies, neither the $(D_\alpha)(A_\beta)$ nor $(D_\beta)(A_\beta)$ types of structures are expected to exhibit appreciable population at 298 K.

All five levels of theory suggest that the $(D_\alpha,D)(A_\alpha,A)g_+$ conformer is the GM at 0 K, where the second D/A in the name indicates an additional hydrogen bond not involving the excess proton.

The related $(D_\alpha,A)(A_\alpha,D)g_-$ conformer lies 1.5 – 3.7 kJ/mol higher at 0 K and is connected to the g_+ conformer by a transition state (TSg_+/g_-) that involves proton transfer between the two hydrazine molecules. Hence, this system lies in a double well potential and because the imaginary frequency is quite high (713 cm^{-1}), the zero-point energy of the TS lies below that of either "stable" conformer. Thus, all levels of theory indicate that TSg_+/g_- is actually the GM at both 0 and 298 K, Table 2. Ignoring the TS, only the M06 level of theory suggests the g_+ conformer is the GM at 298 K. The other levels of theory find the $(D_\alpha,DA)(A_\alpha,DA)$c conformer is the GM at 298 K, with the g_+ conformer being only 1.4 – 2.0 kJ/mol higher in energy. The $(D_\alpha)(A_\alpha)$t conformer is only ~1 kJ/mol higher than the c conformer at 298 K because the lack of the additional hydrogen bonding raises the energy but allows a more flexible structure. Another similar conformer, $(D_\alpha,D)(A_\alpha,A)$c, has one less hydrogen bond than the $(D_\alpha,DA)(A_\alpha,DA)$c conformer shown in Figure 2, which raises its energy by 3.6 – 5.6 kJ/mol at 0 K (11.4 – 13.4 kJ/mol at 298 K). Overall, the relative Gibbs energies of the four low-lying conformers indicate that they are likely to be populated at room temperature. Indeed, a Maxwell-Boltzmann distribution of conformers (using the average Gibbs energy for all levels of theory) suggests populations of 67% for TSg_+/g_-, 28% for c, and 4% for t.

Experimental IRMPD. $(UDMH)_2H^+$. The IRMPD spectrum of $(UDMH)_2H^+$ and the theoretical IR spectra of the four low-lying conformers and the TS are shown in Figure 2. In this system, IRMPD of $(UDMH)_2H^+$ leads exclusively to loss of neutral UDMH to form the $(UDMH)H^+$ ion. Major peaks are found at 790, 920, 1035 (with a shoulder at 990), 1460, 1610, 2895, 2995, 3315, and 3380 cm^{-1}. Comparison with the theoretical spectra indicates that the experimental band at 790 cm^{-1} can be identified as in-phase N–N and N–C stretches of both UDMH molecules, which are then in- and out-of-phase. At 920 cm^{-1} are two bands associated with the NH_2 umbrella motions of these two groups. The smaller peak at 990 cm^{-1} appears to be associated with out-of-phase C–N stretches, and the larger peak at 1035 cm^{-1} corresponds to the NH_2 umbrella motion coupled with a rocking motion of the adjacent CH_3 group on each UDMH. At 1460 cm^{-1}, there is a series of CH_2 bends and the peak at 1610 cm^{-1} is associated with the NH_2 bends in each UDMH molecule. In the 3 μm region, peaks at 2895 and 2995 cm^{-1} are symmetric and asymmetric

CH stretches, respectively. Likewise, the peaks at 3315 and 3380 cm^{-1} are the symmetric and asymmetric NH_2 stretches, respectively.

The major features in the spectrum are reproduced reasonably well by the predicted spectra of any of the $(D_\alpha)(A_\alpha)$ conformers after application of two scaling factors, 0.965 for frequencies in the fingerprint region between 600 and 1800 cm^{-1} and 0.955 for frequencies in the 3 μm region. In the 3 μm region, the TSg_+/g_- spectrum probably does the best job of reproducing the positions and relative intensities of the observed bands. Likewise, this spectrum reproduces the positions of the major bands at 920, 1035, 1460, and 1610 cm^{-1} and a reasonable prediction of their relative intensities, as well as the reduced intensity in the region between 1050 – 1400 cm^{-1}. Other conformers generally predict more intense bands in this region. The TSg_+/g_- spectrum does not predict the band at 790 cm^{-1}, whereas all other conformers do yield a peak in this position. Notably, if we consider the possibility of the four low-lying conformers being populated by the Maxwell-Boltzmann distribution at 298 K noted above (which is dominated by TSg_+/g_-), we find that the resultant IR spectrum recreates the IRMPD spectrum very well, Figure 2.

The three $(D_\alpha)(A_\beta)$ conformers, spectra shown in Figure S1 with structures in Figure S2 (ESI†), also have band positions similar to those of the $(D_\alpha)(A_\alpha)$ conformers with the addition of peaks near 1090 and 1550 cm^{-1}. Although no sharp bands are observed at these wavenumbers, the experimental spectrum does have some intensity in these regions. In contrast, the $(D_\beta)(A_\beta)$ isomers predict substantial intensities above 1625 cm^{-1}, which is inconsistent with experiment, although there is a shoulder of intensity there. Thus, although the low-energy $(D_\alpha)(A_\alpha)$ conformers account for most of the observed spectrum, contributions from higher-lying $(D_\alpha)(A_\beta)$ conformers cannot be excluded on the basis of the experimental spectrum.

Notably, the spectral region just above the fingerprint region probed in these studies may be a better probe of which particular structures are present, but unfortunately is not accessible with the lasers available. According to theory, there is a single band between 1800 and 2300 cm^{-1} corresponding to the proton motion between the two UDMH molecules. This proton motion is very sensitive to the extent of hydrogen-bonding and varies from 2263, 1862, 2069, and 1957 cm^{-}

[1] for the $(D_\alpha)(A_\alpha)$ g_+, g_-, c, and t conformers, respectively (all scaled by 0.965). However, this proton motion is often subject to large anharmonic shifts,[59, 60] which could shift the position from these predicted harmonic band positions. Significant broadening can also occur, but is not always observed,[59-62] potentially consistent with the observation of non-zero intensity at the edges (1800 and 2800 cm^{-1}) of the present spectrum. Both effects could require advanced theoretical methods to properly interpret.[63, 64]

Theoretical Structures. $(N_2H_4)_2H^+$. Similar to the proton-bound UDMH dimer case, the theoretical conformers of the proton-bound hydrazine dimer were examined in detail in previous work.[15] Our nomenclature indicates whether the protonated and neutral hydrazine molecules donate (D) or accept (A) a hydrogen bond from both nitrogen atoms. In addition, the ∠NNNN dihedral angle through the shared proton is specified by using c, g, t, and + or – for the gauche angles when needed to distinguish similar conformers. The four low-lying conformers located for the proton-bound hydrazine dimer are shown in Figure 3, with relative energies in Table 3. All five levels of theory suggest the (D,D)(A,A)g_+ conformer is the GM at 0 K and also at 298 K for the M06 and MP2(full) levels of theory. At 298 K, the PBE0 level of theory suggests the (DD,A)(A,AD)$g_–$ conformer is the GM, B3LYP indicates (D,DA)(A,DA)c is the GM, and mPW1PW91 indicates (D,D)(A,A)t is the 298 K GM. In these four conformers (which will be abbreviated as g_+, $g_–$, c, and t below), the average short NH bond to the shared proton is 1.11 Å, whereas the average long NH bond is 1.58 Å. All four conformers have additional H-bonding interactions ranging in length from 2.29 to 2.88 Å.

Interconversion among these conformers was also explored theoretically. After ZPE and thermal corrections, TSg_+/$g_–$ (where the imaginary frequency corresponds primarily to the high frequency proton exchange between the two hydrazine molecules) becomes lower in energy than either g_+ or $g_–$. The t and c conformers are coupled by TSt/c, which lies 4.6 – 10.5 kJ/mol higher in energy at 298 K. Because the average internal energy of this complex at 298 K is 28.6 kJ/mol, interchange between these conformers is possible at room temperature. In contrast, TSg_+/c and TS$g_–$/t are sufficiently high in energy, > 9 kJ/mol, that interchange between the g_+ and c conformers

and the g_- and t conformers is unlikely at room temperature. A Maxwell–Boltzmann population distribution at 298 K for the TSg_+/g_-, c, and t conformers is 80, 11, and 9%, respectively, using the average relative Gibbs energies.

Experimental IRMPD. $(N_2H_4)_2H^+$. The comparisons between the IRMPD spectrum and computed IR spectra for these four conformations and TSg_+/g_- of $(N_2H_4)_2H^+$ are shown in Figure 3. Here, a scaling factor of 0.975 was used at low frequencies and 0.955 at high frequencies. The optimum range for the low frequency scaling factor varies with the conformer, 600 – 1470 cm^{-1} was used for the TS, c, and t conformers, whereas g_+ and g_- reproduced the IRMPD spectrum better if the range extended to 1800 cm^{-1}. In this system, IRMPD of $(N_2H_4)_2H^+$ leads exclusively to loss of neutral N_2H_4 forming the $N_2H_5^+$ ion. The bands calculated for TSg_+/g_- agree reasonably well with the experimental spectrum throughout the ranges examined although the intensities in the 800 – 1300 cm^{-1} range are somewhat high. A band predicted at 640 cm^{-1} is not observed, although this is potentially because the laser power drops off here and the low energy of these photons means more are needed for dissociation. Notably, this TS has an intense band at 1250 cm^{-1} that is not found in the other four conformers. This corresponds to motion of the shared proton coupled with $N_\alpha H$ bends. The presence of this band would explain the intensity observed experimentally at this frequency (especially if the band were more diffuse). As noted above, contributions from all the conformers are possible and an overlaid spectrum corresponding to the Maxwell-Boltzmann distribution calculated above is shown in Figure 3. This overlaid spectrum reproduces the experimental spectrum fairly well, including better reproduction of the relative intensities.

The experimental band at 890 cm^{-1} can be identified as the NH_2 umbrella motion of the two neutral NH_2 moieties. At 1060 cm^{-1}, the NH_2 umbrella motions are coupled with the adjoining covalent N–N stretch. The 1130 cm^{-1} peak is associated with HNNH bends, as is the band at 1380 cm^{-1}. The unique band in the TS at 1250 cm^{-1} can be identified as NNH bends coupled with motion of the shared proton. The intense peak at 1605 cm^{-1} is associated with the NH_2 scissor bends. The single experimental band observed in the 3 μm region extends from 3250 – 3450 cm^{-1} and

corresponds to various NH stretches.

Protonation Site and Structural Trends. Our results indicate that in $(UDMH)H^+$, the proton binds to the methylated nitrogen atom, which is favored over the unmethylated nitrogen because of its higher gas phase basicity resulting from the electron donating methyl groups. This is consistent with the $(UDMH)H^+$ isomer protonated at the unmethylated nitrogen atom having a much higher calculated energy. Formation of this latter isomer can be ruled out on the basis of the comparison between the calculated and experimental spectra (*vide supra*). In the $(UDMH)_2H^+$ dimer, the calculated lowest energy isomers have the proton shared between the methylated nitrogen atoms of the two UDMH monomers. This can again be attributed to proton binding to the methylated nitrogen atoms being favored because of their larger gas phase basicity compared with that of the unmethylated nitrogen atoms. Although the monomer units for $(UDMH)_2H^+$ are asymmetrical and those of the hydrazine dimer, $(N_2H_4)_2H^+$, are symmetrical, our results indicate that these two protonated dimers share similarities in the structures of their lowest energy isomers. Interestingly, the GM structure for both dimer complexes is found to be TSg_+/g_-, a transition state that involves proton transfer between the monomers. For $(UDMH)_2H^+$, the two stable structures, $(D_\alpha,D)(A_\alpha,A)g_+$ and $(D_\alpha,A)(A_\alpha,D)g_-$, that are bridged by this TS are slightly higher in energy than two other low-lying conformers, $(D_\alpha,DA)(A_\alpha,DA)c$ and $(D_\alpha)(A_\alpha)t$. For $(N_2H_4)_2H^+$, the analogous four conformers generally have similar Gibbs energies that are somewhat higher than the GM TSg_+/g_- structure. Variations in the energies of these lowest-energy conformers found for $(UDMH)_2H^+$ and $(N_2H_4)_2H^+$ can be attributed to differences in the number of hydrogen bonds that can be formed and the effects of methylation on the gas phase basicity of the nitrogen atoms. For both dimer complexes, the largest contribution to the calculated composite spectrum comes from the GM TS structure with relative populations of 80 and 67% for $(N_2H_4)_2H^+$ and $(UDMH)_2H^+$, respectively. The $(D_\alpha,DA)(A_\alpha,DA)c$ structure of $(UDMH)_2H^+$ contributes 28% to the composite spectrum, whereas the analogous (D,DA)(A,DA)c structure of $(N_2H_4)_2H^+$, with the same number of hydrogen bonds, contributes 11% to the composite spectrum. The relatively higher stability of the $(D_\alpha,DA)(A_\alpha,DA)c$ structure of $(UDMH)_2H^+$ may arise from a stronger interaction of the shared

proton because of the methylated nitrogen atoms, which could give rise to stronger hydrogen bonds. The $(D_\alpha)(A_\alpha)$t conformer of $(UDMH)_2H^+$ contributes 4% to the composite spectrum, whereas the analogous (D,D)(A,A)t conformer of $(N_2H_4)_2H^+$ contributes 9% to the composite spectrum. Here, the higher relative stability of the (D,D)(A,A)t conformer of $(N_2H_4)_2H^+$ can be attributed to a hydrogen bond that is present and cannot be formed in the $(D_\alpha)(A_\alpha)$t conformer of $(UDMH)_2H^+$ because of the methylated nitrogen atoms.

Conclusions

The gas-phase structures of $(UDMH)H^+$, $(UDMH)_2H^+$, and $(N_2H_4)_2H^+$ are examined by IRMPD action spectroscopy utilizing light generated by the free electron laser FELIX and an OPO. Comparisons of the measured IRMPD spectra to linear absorption spectra calculated at the B3LYP-GD3BJ/6-311+G(d,p) level of theory show that the proton on $(UDMH)H^+$ clearly prefers binding to the methylated nitrogen atom (α) over the un-methylated nitrogen atom (β), yet the preferred α conformer could not be determined on the basis of the IRMPD spectrum alone. For $(UDMH)_2H^+$, the overlaid spectrum associated with a Maxwell-Boltzmann population of low-lying conformeric species reproduces the IRMPD spectrum very well over the collected spectral range, which suggests that multiple low-lying conformers are populated in the experiment. Higher-lying $(D_\alpha)(A_\beta)$ conformers of $(UDMH)_2H^+$ cannot be ruled out on the basis the observed IRPMD spectrum. For $(N_2H_4)_2H^+$, four low-lying conformers reproduce the collected IRMPD spectrum well, suggesting again that multiple conformers are probably populated at 298 K.

Finally, it is worth commenting on the ability of theory to describe protonated hydrazine and UDMH, and their clusters. As noted in the introduction, the ability to predict the likely low-energy structures of similar complexes could be a more discerning approach to determining which level of theory is most accurate than the comparison of bond energies made in previous work. However, for the two proton-bound dimers, all levels of theory yielded similar predictions and the spectra are consistent with a fairly broad distribution of low-lying conformers. In contrast, for protonated UDMH, the experimental spectrum agrees best with the low-lying α(t,g) conformer,

where a B3LYP-GD3BJ approach yielded the lowest energy prediction, but the experimental spectrum is consistent with contributions from both α(g,g) (the GM) and α(t,g). Taken as a whole, our spectroscopic results on hydrazines do not yield a clear-cut recommendation for a particularly useful level of theory.

Associated Content

Electronic Supplementary Material (ESI) available**:** Figure containing the comparison between the IRMPD spectrum of $(UDMH)_2H^+$ and the higher-lying isomers of $(UDMH)_2H^+$.

Author Information

Corresponding Author

P. B. Armentrout – armentrout@chem.utah.edu; ORCID: 0000-0003-2953-6039

Conflicts of Interest

The authors declare no conflicts.

Acknowledgements

This work was supported by ENSCO Inc. and the National Science Foundation, Grants No. CHE-1709789 (MTR), CHE-1954142 (PBA), and OISE-1357787. We thank the Center of High Performance Computing at the University of Utah for the generous allocation of computer time and the *Nederlandse Organisatie voor Wetenschappelijk Onderzoek* (NWO) for the support of the FELIX Laboratory.

References

1. M. Zheng, R. Cheng, X. Chen, N. Li, L. Li, X. Wang and T. Zhang, *Int. J. Hydrogen Energy*, 2005, **30**, 1081-1089.
2. S. G. Pakdehi, M. Salimi and M. Rasoolzadeh, *Res. Appl. Mech. Eng.*, 2014, **3**, 21-25.
3. J.-P. Schirmann and P. Bourdauducq, *Ullmann's Encyclopedia of Industrial Chemistry*, 2000.

4. J. A. Gardner, R. A. Dressler, R. H. Salter and E. Murad, *J. Phys. Chem.*, 1992, **96**, 4210-4217.
5. G. Lunn, E. B. Sansone and L. K. Keefer, *Environmental Science & Technology*, 1983, **17**, 240-243.
6. E. C. Tuazon, W. P. L. Carter, A. M. Winer and J. N. Pitts, *Environmental Science & Technology*, 1981, **15**, 823-828.
7. U. Buck, X. Gu, M. Hobein and C. Lauenstein, *Chem. Phys. Lett.*, 1989, **163**, 455-460.
8. S. Schneider, T. Hawkins, Y. Ahmed, S. Deplazes and J. Mills, in *Ionic Liquids: Science and Applications*, American Chemical Society, 2012, vol. 1117, ch. 1, pp. 1-25.
9. Y. Zhang, H. Gao, Y. Guo, Y.-H. Joo and J. n. M. Shreeve, *Chemistry – A European Journal*, 2010, **16**, 3114-3120.
10. T. M. Klapötke and J. Stierstorfer, *J. Am. Chem. Soc.*, 2009, **131**, 1122-1134.
11. B. D. Prince, B. A. Fritz and Y.-H. Chiu, in *Ionic Liquids: Science and Applications*, American Chemical Society, 2012, vol. 1117, ch. 2, pp. 27-49.
12. B. R. Donius and J. L. Rovey, *Journal of Spacecraft and Rockets*, 2011, **48**, 110-123.
13. S. P. Berg and J. L. Rovey, *Journal of Spacecraft and Rockets*, 2017, **54**, 592-601.
14. C. P. McNary and P. B. Armentrout, *J. Chem. Phys.*, 2016, **145**, 214311.
15. C. P. McNary and P. B. Armentrout, *J. Phys. Chem. A*, 2016, **120**, 9690-9701.
16. C. P. McNary and P. B. Armentrout, *J. Chem. Phys.*, 2017, **147**, 124306.
17. J. Oomens, B. G. Sartakov, G. Meijer and G. von Helden, *Int. J. Mass Spectrom.*, 2006, **254**, 1-19.
18. N. C. Polfer and J. Oomens, *Mass Spectrom. Rev.*, 2009, **28**, 468−494.
19. N. C. Polfer and J. Oomens, *Phys. Chem. Chem. Phys.*, 2007, **9**, 3804-3817.
20. J. S. Prell, T. M. Chang, J. A. Biles, G. Berden, J. Oomens and E. R. Williams, *J. Phys. Chem. A*, 2011, **115**, 2745-2751.
21. A. M. Rijs and J. Oomens, *Top. Curr. Chem.*, 2015, **364**, 1-42.
22. D. Oepts, A. F. G. van der Meer and P. W. van Amersfoort, *Infrared Phys. Technol.*, 1995, **36**, 297-308.
23. J. Martens, G. Berden, C. R. Gebhardt and J. Oomens, *Rev. Sci. Instrum.*, 2016, **87**, 103108.
24. L. A. Hamlow, Y. Zhu, Z. J. Devereaux, N. A. Cunningham, G. Berden, J. Oomens and M. T. Rodgers, *J. Am. Soc. Mass Spectrom.*, 2018, **29**, 2125-2137.
25. W. A. Donald, G. N. Khairallah and R. A. J. O'Hair, *J. Am. Soc. Mass Spectrom.*, 2013, **24**, 811-815.
26. S. Gronert, *J. Am. Soc. Mass Spectrom.*, 1998, **9**, 845-848.
27. N. C. Polfer, J. Oomens, D. T. Moore, G. von Helden, G. Meijer and R. C. Dunbar, *J. Am. Chem. Soc.*, 2006, **128**, 517-525.
28. J. J. Valle, J. R. Eyler, J. Oomens, D. T. Moore, A. F. G. van der Meer, G. von Heldon, G. Meijer, C. L. Hendrickson, A. G. Marshall and G. T. Blakney, *Rev. Sci. Instrum.*, 2005, **76**, 023103.
29. L. A. Posey, M. J. Deluca and M. A. Johnson, *Chem. Phys. Lett.*, 1986, **131**, 170-174.
30. S. Guan and A. G. Marshall, *Int. J. Mass Spectrom. Ion Processes*, 1996, **157-158**, 5-37.
31. A. G. Marshall, T. C. L. Wang and T. L. Ricca, *J. Am. Chem. Soc.*, 1985, **107**, 7893-7897.
32. R. C. Dunbar, *J. Chem. Phys.*, 1989, **90**, 7369-7375.
33. A. D. Becke, *J. Chem. Phys.*, 1993, **98**, 5648-5652.
34. R. Ditchfield, W. J. Hehre and J. A. Pople, *J. Chem. Phys.*, 1971, **54**, 724-728.
35. S. Grimme, S. Ehrlich and L. Goerigk, *J. Comput. Chem.*, 2011, **32**, 1456-1465.

36. Y. Zhao and D. G. Truhlar, *Theor. Chem. Acc.*, 2008, **120**, 215-241.
37. J. P. Perdew, K. Burke and M. Ernzerhof, *Phys. Rev. Lett.*, 1997, **78**, 1396-1396.
38. C. Adamo and V. Barone, *J. Chem. Phys.*, 1999, **110**, 6158-6170.
39. C. Adamo and V. Barone, *Chem. Phys. Lett.*, 1997, **274**, 242-250.
40. C. Adamo and V. Barone, *J. Chem. Phys.*, 1998, **108**, 664-675.
41. C. Möller and M. S. Plesset, *Phys. Rev.*, 1934, **46**, 618-622.
42. M. J. Frisch, M. Head-Gordon and J. A. Pople, *Chem. Phys. Lett.*, 1990, **166**, 275-280.
43. M. J. Frisch, M. Head-Gordon and J. A. Pople, *Chem. Phys. Lett.*, 1990, **166**, 281-289.
44. M. Head-Gordon and T. Head-Gordon, *Chem. Phys. Lett.*, 1994, **220**, 122-128.
45. M. Head-Gordon, J. A. Pople and M. J. Frisch, *Chem. Phys. Lett.*, 1988, **153**, 503-506.
46. S. Grimme, J. Antony, S. Ehrlich and H. Krieg, *J. Chem. Phys.*, 2010, **132**, 154104-154119.
47. J. Čížek, in *Adv. Chem. Phys.*, John Wiley & Sons, Inc., 2007, DOI: 10.1002/9780470143599.ch2, pp. 35-89.
48. G. D. Purvis and R. J. Bartlett, *J. Chem. Phys.*, 1982, **76**, 1910-1918.
49. G. E. Scuseria, C. L. Janssen and H. F. Schaefer, *J. Chem. Phys.*, 1988, **89**, 7382-7387.
50. G. E. Scuseria and H. F. Schaefer, *J. Chem. Phys.*, 1989, **90**, 3700-3703.
51. J. A. Pople, M. Head-Gordon and K. Raghavachari, *J. Chem. Phys.*, 1987, **87**, 5968-5975.
52. J. M. L. Martin, *Chem. Phys. Lett.*, 1996, **259**, 669-678.
53. M. T. Rodgers and P. B. Armentrout, *Int. J. Mass Spectrom.*, 2007, **267**, 167-182.
54. J. K. Martens, J. Grzetic, G. Berden and J. Oomens, *Int. J. Mass Spectrom.*, 2015, **377**, 179-187.
55. Y.-w. Nei, N. Hallowita, J. D. Steill and J. R. Oomens, M. T. , *J. Phys. Chem. A*, 2013, **117**, 1319-1335.
56. R. R. Wu, C. C. He, L. A. Hamlow, Y.-w. Nei, G. Berden, J. Oomens and M. T. Rodgers, *J. Phys. Chem. B*, 2016, **120**, 4616-4624.
57. C. F. Correia, P. O. Balaj, D. Scuderi, P. Maitre and G. Ohanessian, *J. Am. Chem. Soc.*, 2008, **130**, 3359-3370.
58. R. R. Wu, C. C. He, L. A. Hamlow, Y.-w. Nei, G. Berden, J. Oomens and M. T. Rodgers, *Phys. Chem. Chem. Phys.*, 2016, **18**, 15081-15090.
59. J. M. Headrick, E. G. Diken, R. S. Walters, N. I. Hammer, R. A. Christie, J. Cui, E. M. Myshakin, M. A. Duncan, M. A. Johnson and K. D. Jordan, *Science*, 2005, **308**, 1765-1769.
60. J. R. Roscioli, L. R. McCunn and M. A. Johnson, *Science*, 2007, **316**, 249-254.
61. D. A. Thomas, M. Marianski, E. Mucha, G. Meijer, M. A. Johnson and G. von Helden, *Angew. Chem. Int. Ed.*, 2018, **57**, 10615-10619.
62. N. Heine and K. Asmis, *Int. Rev. Phys. Chem.*, 2014, **34**, 1-34.
63. L. C. Dzugan, R. J. DiRisio, L. R. Madison and A. B. McCoy, *Faraday Discuss.*, 2018, **212**, 443-466.
64. X. Cheng and R. P. Steele, *J. Chem. Phys.*, 2014, **141**, 104105.

Table 1. Relative energies at 0 K (Gibbs energies at 298 K) in kJ/mol for conformers and isomers of protonated UDMH[a]

Structure	B3LYP-GD3BJ	ROMP2(Full)	ROCCSD(T)[b]
α(g,g)	0.0 (0.0)	0.0 (0.0)	0.0 (0.0)
TS(g-t,g)	9.4 (10.1)	11.7 (12.5)	10.5 (11.3)
α(t,g)	1.3 (1.2)	2.9 (2.7)	2.2 (2.1)
TSα/β	187.5 (186.8)	194.4 (193.7)	194.2 (193.5)
β	28.9 (28.7)	35.1 (34.9)	32.2 (32.0)

[a] Gibbs energies in parentheses. All values calculated at the level of theory indicated using the 6-311+G(2d,2p) basis set with optimized structures, zero-point energies, and thermal corrections calculated at B3LYP-GD3BJ/6-311+G(d,p) level of theory. [b] ROCCSD(T)/Feller CBS//B3LYP-GD3BJ/6-311+G(d,p).

Table 2. Relative energies at 0 K (Gibbs energies at 298 K) in kJ/mol for low-lying conformers and isomers of the proton-bound UDMH dimer[a]

Structures	B3LYP	M06	mPW1PW91	PBE0	MP2(full)
$(D_\alpha,D)(A_\alpha,A)g_+$	**0.0** (1.8)	**0.0 (0.0)**	**0.0** (2.0)	**0.0** (1.8)	**0.0** (1.4)
TSg_+/g_-	-3.3 (-1.3)	-2.6 (-2.3)	-3.8 (-1.5)	-5.3 (-3.3)	-3.4 (-1.8)
$(D_\alpha,A)(A_\alpha,D)g_-$	2.1 (2.6)	3.7 (2.5)	1.7 (2.4)	1.5 (2.1)	2.3 (2.5)
$(D_\alpha,DA)(A_\alpha,DA)c$	0.3 **(0.0)**	2.6 (0.5)	0.1 **(0.0)**	0.3 **(0.0)**	0.7 **(0.0)**
$(D_\alpha)(A_\alpha)t$	4.5 (1.0)	6.2 (0.9)	4.2 (1.0)	4.3 (0.9)	4.9 (1.0)
$(D_\alpha,D)(A_\alpha,A)c$	9.4 (13.8)	9.8 (12.3)	9.1 (13.7)	9.9 (14.3)	8.7 (12.7)
$(D_\alpha,D)(A_\beta,A)g$	6.0 (6.8)	4.1 (3.2)	4.7 (5.8)	6.3 (7.2)	8.4 (8.9)
$(D_\alpha,D)(A_\beta,A)c$	7.0 (6.9)	5.9 (3.5)	4.9 (5.1)	7.1 (7.1)	9.5 (9.1)
$(D_\alpha)(A_\beta)t$	10.7 (8.0)	10.1 (5.6)	7.2 (4.8)	10.2 (7.6)	14.5 (11.4)
$(D_\beta)(A_\beta)g$	29.5 (29.4)	25.9 (24.1)	21.8 (22.0)	25.9 (25.9)	40.1 (39.7)
$(D_\beta)(A_\beta)c$	28.3 (29.4)	25.3 (24.6)	21.7 (23.0)	24.7 (25.8)	38.3 (39.0)
$(D_\beta)(A_\beta)t$	32.3 (27.7)	29.6 (23.3)	22.6 (18.3)	28.9 (24.4)	41.3 (36.4)

[a]Taken from previous work.[15] Gibbs energies in parentheses. Global minimum in bold. All values calculated at the level of theory indicated with empirical dispersion included for B3LYP, M06, and PBE0 levels of theory using the 6-311+G(2d,2p) basis set with structures, zero-point energies, and thermal energies calculated at B3LYP-GD3BJ/6-311+G(d,p) level of theory.

Table 3. Relative energies at 0 K (Gibbs energies at 298 K) in kJ/mol of low-lying conformers of protonated hydrazine dimer[a]

Structures	B3LYP	M06	mPW1PW91	PBE0	MP2(full)
(D,D)(A,A)g_+	**0.0** (0.3)	**0.0 (0.0)**	**0.0** (2.1)	**0.0** (1.0)	**0.0 (0.0)**
TSg_+/g_-	-3.4 (-3.6)	-2.7 (-3.1)	-5.7 (-6.0)	-5.6 (-6.0)	-1.4 (-1.8)
(DD,A)(A,AD)g_-	1.9 (0.2)	3.6 (1.5)	0.5 (0.5)	1.0 **(0.0)**	2.1 (0.8)
(DD)(A,A)t	4.5 (0.6)	7.8 (3.6)	2.2 **(0.0)**	3.9 (0.7)	5.1 (0.9)
(D,DA)(A,DA)c	0.8 **(0.0)**	2.6 (1.6)	0.3 (1.3)	0.7 (0.7)	1.5 (0.5)

[a] Taken from previous work.[15] Gibbs energies in parentheses. Global minimum in bold. All values calculated at the level of theory indicated with empirical dispersion included for B3LYP, M06, and PBE0 levels of theory using the 6-311+G(2d,2p) basis set with structures, zero-point energies, and thermal energies calculated at B3LYP-GD3BJ/6-311+G(d,p) level of theory.

Figure Captions

Figure 1. IRMPD spectrum of $(UDMH)H^+$ compared to the IR spectra for the two low-lying (α) and one higher-lying (β) isomers of $(UDMH)H^+$. Relative 298 K Gibbs energies in kJ/mol at the B3LYP-GD3BJ, MP2, and CCSD(T) levels are also provided. Two scaling factors were used: 0.975 for frequencies below 1275 cm^{-1} (red) and 0.955 for frequencies above 1275 cm^{-1} (blue). The bottom panel shows the IR spectrum of the α(g,g) and α(t,g) conformers convoluted together on the basis of their Maxwell-Boltzmann population at 298 K using the Gibbs energies from B3LYP-GD3BJ calculations.

Figure 2. IRMPD spectrum of $(UDMH)_2H^+$ compared to the IR spectra for the four low-lying conformers of $(UDMH)_2H^+$ and one transition state between them. Relative 298 K Gibbs energies in kJ/mol at the B3LYP, M06, mPW1PW91, PBE0, and MP2 levels are also provided. Two scaling factors were used: 0.965 for frequencies below 1800 cm^{-1} (red) and 0.955 for frequencies above 1800 cm^{-1} (blue). The bottom panel shows the IR spectrum of the TSg_+/g_-, $(D_\alpha,DA)(A_\alpha,DA)c$, and $(D_\alpha)(A_\alpha)t$ conformers convoluted together on the basis of their Maxwell-Boltzmann population at 298 K using the average Gibbs energy from all calculations.

Figure 3. IRMPD spectrum of $(N_2H_4)_2H^+$ compared to the IR spectra for the four low-lying conformers of $(N_2H_4)_2H^+$ and one transition state between them. Relative 298 K Gibbs energies in kJ/mol at the B3LYP, M06, mPW1PW91, PBE0, and MP2 levels are also provided. Two scaling factors were used: 0.975 for low frequencies (red) and 0.955 for high frequencies (blue). The bottom panel shows the IR spectrum of the TSg_+/g_-, (D,DA)(A,DA)c, and (DD)(A,A)t conformers convoluted together on the basis of their Maxwell-Boltzmann population at 298 K using the average Gibbs energy from all calculations.

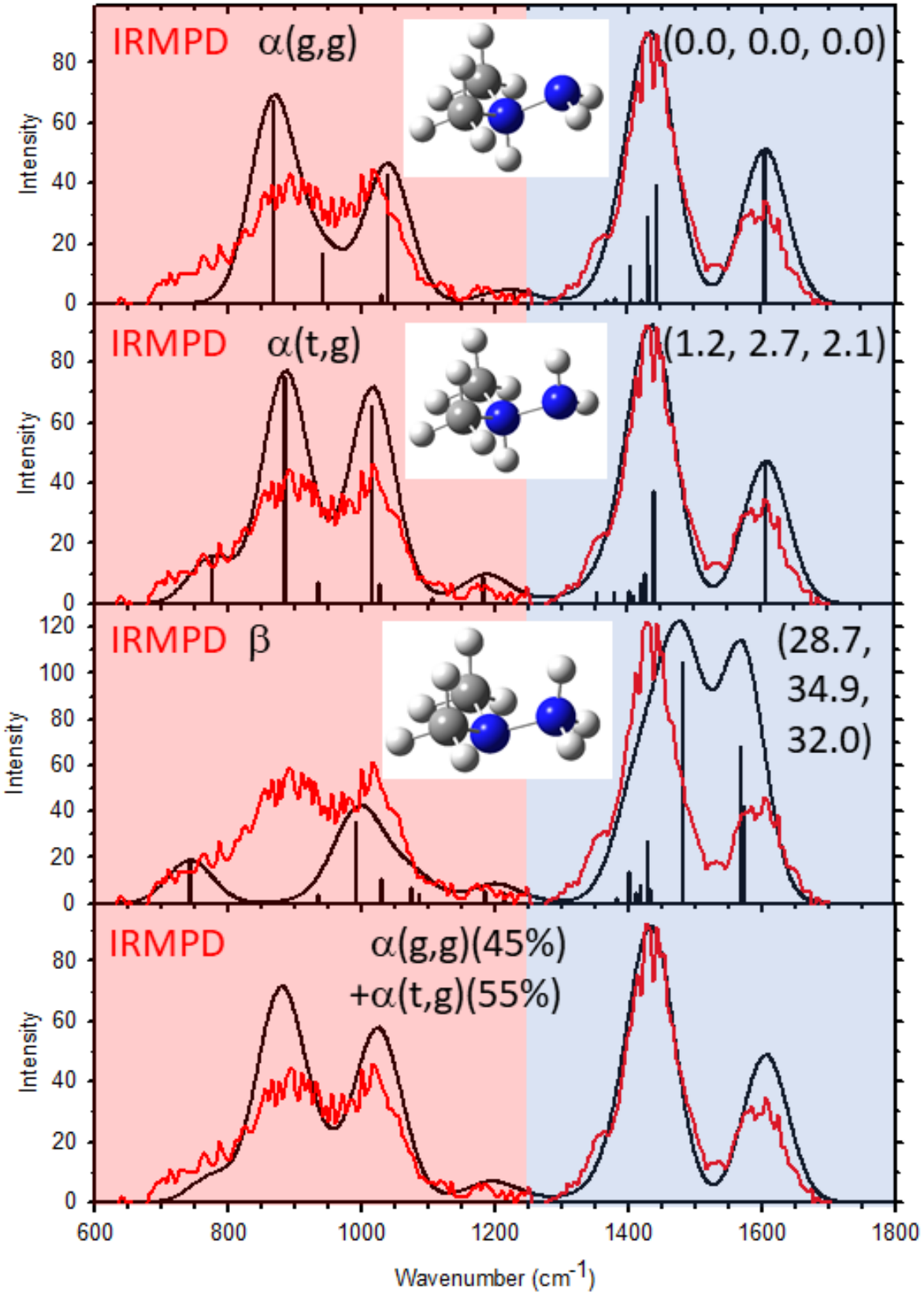
IRMPD α(g,g)
(0.0, 0.0, 0.0)
IRMPD α(t,g)
(1.2, 2.7, 2.1)
IRMPD β
(28.7, 34.9, 32.0)
IRMPD
α(g,g)(45%)
+α(t,g)(55%)
Intensity
Wavenumber (cm-1)

Figure 1

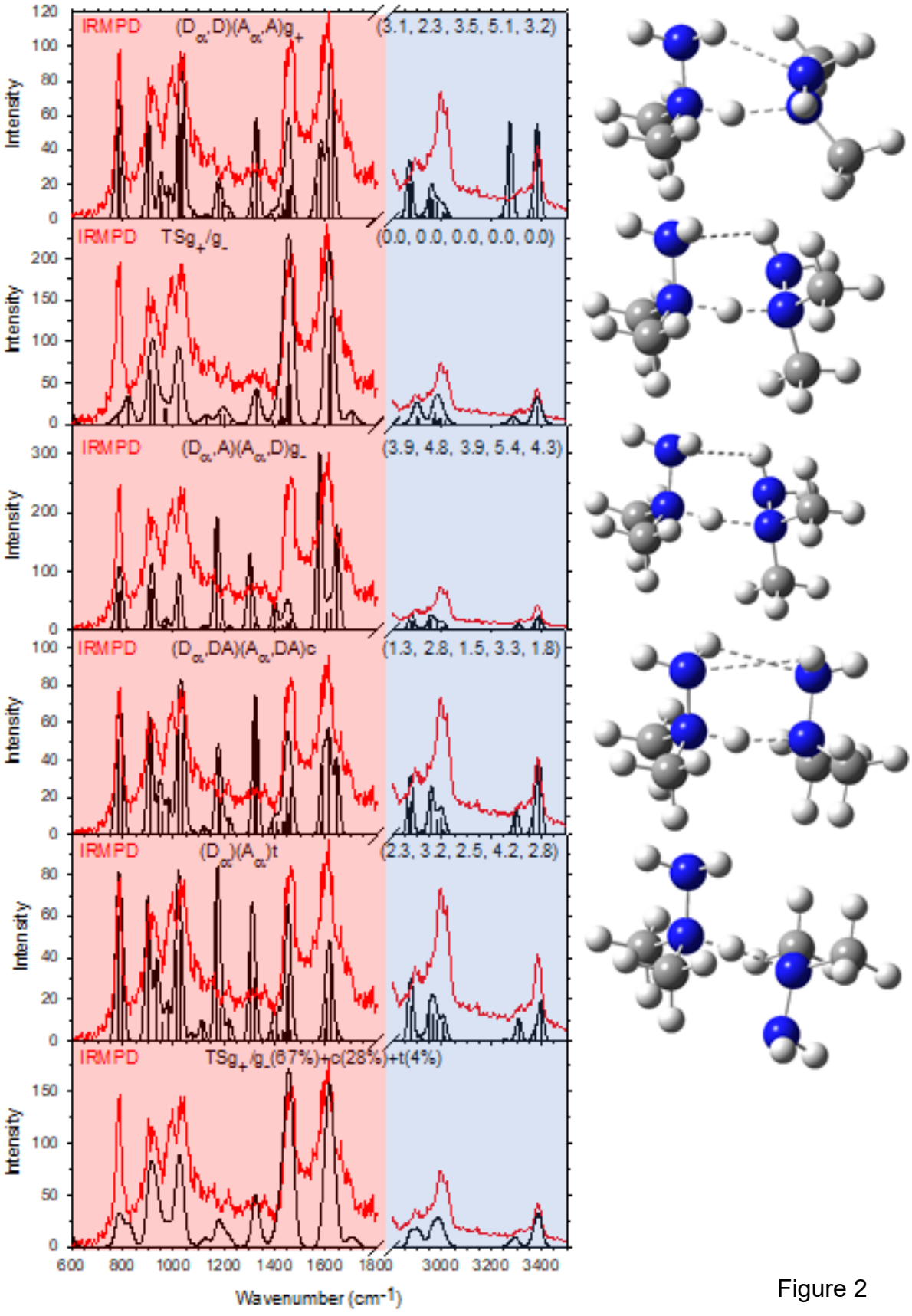
IRMPD
(Dα,D)(Aα,A)g+
(3.1, 2.3, 3.5, 5.1, 3.2)
IRMPD
TSg+/g-
(0.0, 0.0, 0.0, 0.0, 0.0)
IRMPD
(Dα,A)(Aα,D)g-
(3.9, 4.8, 3.9, 5.4, 4.3)
IRMPD
(Dα,DA)(Aα,DA)c
(1.3, 2.8, 1.5, 3.3, 1.8)
IRMPD
(Dα)(Aα)t
(2.3, 3.2, 2.5, 4.2, 2.8)
IRMPD
TSg+/g-(67%)+c(28%)+t(4%)
Intensity
Wavenumber (cm-1)

Figure 2

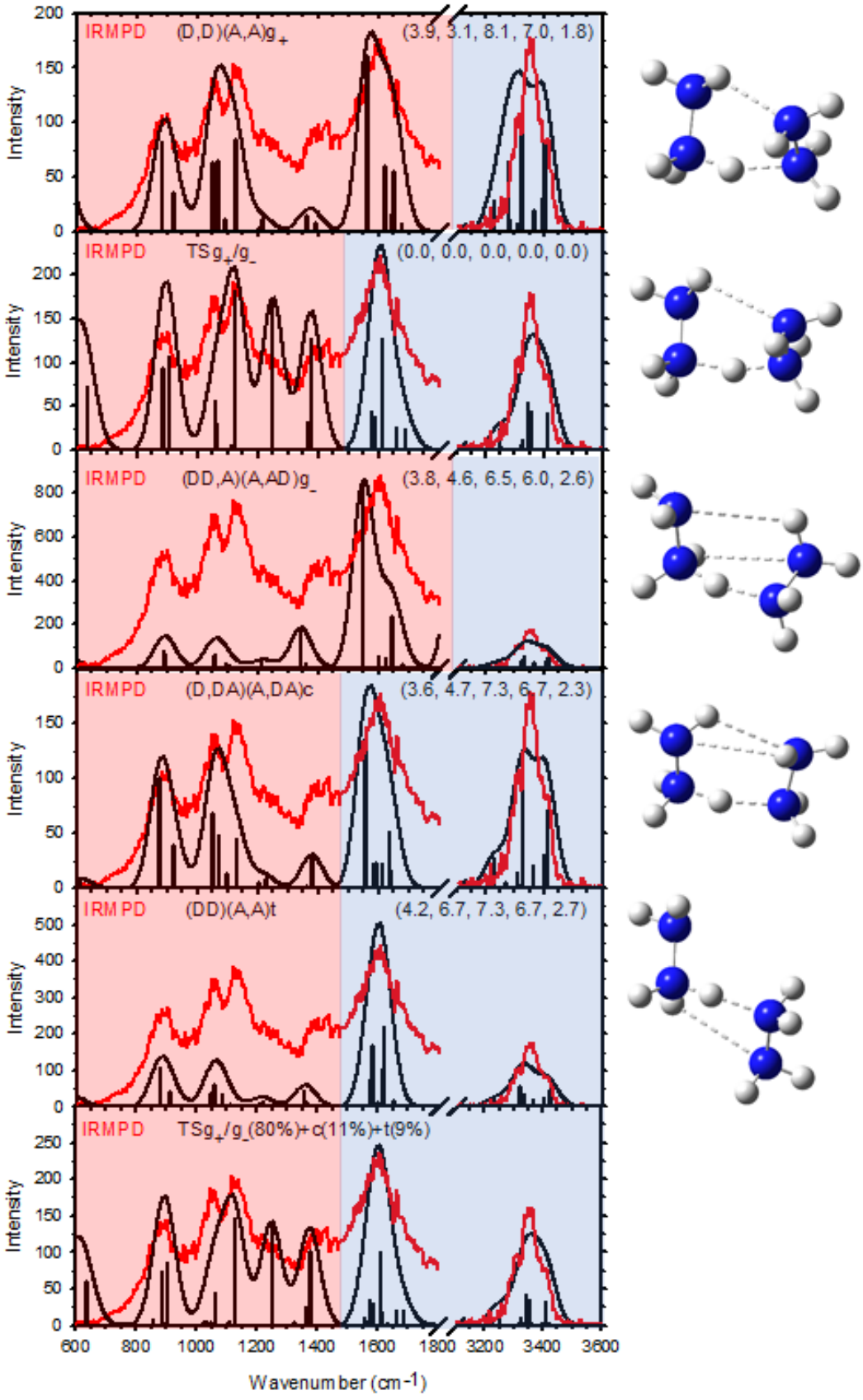
IRMPD (D,D)(A,A)g+ (3.9, 3.1, 8.1, 7.0, 1.8)
IRMPD TSg+/g- (0.0, 0.0, 0.0, 0.0, 0.0)
IRMPD (DD,A)(A,AD)g- (3.8, 4.6, 6.5, 6.0, 2.6)
IRMPD (D,DA)(A,DA)c (3.6, 4.7, 7.3, 6.7, 2.3)
IRMPD (DD)(A,A)t (4.2, 6.7, 7.3, 6.7, 2.7)
IRMPD TSg+/g-(80%)+c(11%)+t(9%)
Intensity
Wavenumber (cm-1)

Figure 3